NASA Technical Memorandum 83507

Complexities of High Temperature Metal Fatigue—Some Steps Toward Understanding

S. S. Manson
Case Western Reserve University
Cleveland, Ohio

and

G. R. Halford
Lewis Research Center
Cleveland, Ohio

Presented at the
Twenty-fifth Annual Israeli Conference on Aeronautics and Astronautics
sponsored by the University of Haifa
Haifa, Israel, February 23–25, 1983

NASA

COMPLEXITIES OF HIGH TEMPERATURE METAL FATIGUE - SOME STEPS TOWARD UNDERSTANDING

S. S. Manson
Case Western Reserve University
Cleveland, Ohio 44106

and

G. R. Halford
National Aeronautics and Space Administration
Lewis Research Center
Cleveland, Ohio 44135

E-1852

SUMMARY

After pointing out many of the complexities that attend high temperature metal fatigue beyond those already studied in the sub-creep range, a description of the micromechanisms of deformation and fracture is presented for several classes of materials that have been studied over the past dozen years. Strainrange Partitioning (SRP) is used as a framework for interpreting the results. Several generic types of behavior have been observed with regard both to deformation and fracture and each is discussed in the context of the micromechanisms involved.

Treatment of cumulative fatigue damage and the possibility of "healing" of damage in successive loading loops, has led to a new interpretation of the Interaction Damage Rule of SRP. Using the concept of "equivalent micromechanistic damage" -- that the same damage on a microscopic scale is induced if the same hysteresis loops are generated, element for element -- it turns out the Interaction Damage Rule essentially compounds a number of variants of hysteresis loops, all of which have the same damage according to SRP concepts, into a set of loops each containing only one of the generic SRP strainranges. Thus the damage associated with complex loops comprising several types of strainrange can be analyzed by considering a combination of loops each containing only one type of strainrange. This concept is expanded to show how several independent loops can combine to "heal" creep damage in a complex loading history. Experimental data to verify these concepts are presented for limited cases. The cumulative damage effect of interaction of high cycle fatigue with low cycle fatigue is also touched on briefly, and some experimental data are presented.

Finally, brief mention is made of a recent study comparing creep rates in tension and compression for 316 SS in which it is found that at the same stress level and temperature creep rate in compression is much lower than in tension. This result has important implications in relation to current extensive efforts in constitutive modeling for high temperature fatigue.

INTRODUCTION

In 1964 the first author presented before the Society for Experimental Stress Analysis a paper entitled "Fatigue: A Complex Subject -- Some Simple

Approximations (ref. 1). Its theme was to point to the immense complexity that attends the fatigue process and yet to explain that simple useful relations have evolved, suitable for engineering application through a recognition of the primary and relegating others as contributory but secondary. The Universal Slopes Equation highlighted in the lecture, which placed primary importance on strain range as the governing variable, and which showed how ductility and tensile strength influenced the ability of a material to absorb strain reversals has found many useful applications in design against fatigue.

It was not much later that he began to be concerned more deeply with metal fatigue at high temperatures. In 1965, for the First International Conference on Fatigue and Fracture, he was invited to give a lecture on "Interfaces Between Creep, Fatigue and Fracture" (ref. 2). While trying to find a link between creep and fatigue, it occurred that it might be possible to incorporate into the Universal Slopes Equation the essential difference observed between fatigue in the creep range and that below this range. This difference, the presence and absence of intercrystalline fracture, could be interpreted in terms of the number of cycles required to initiate a crack. Thus the early development of an intergranular crack, either by some creep mechanism or by environmental attack, had the effect of by-passing the number of cycles required to initiate a crack by the normal fatigue mechanism. Fatigue life could therefore become substantially lower. The reduction was by about a factor of 10--thus the 10 percent Rule of the "Interfaces" paper provided an interim engineering approach that is, in fact still useful for first approximation calculations.

But as further research embraced more materials and more variables in loading history it became clear that an approach as simple as the 10 percent Rule could not be the whole answer. Even after patching it up to take further variables into account it was still not sufficiently broad a concept for general application. The next 15 years or so saw many new methods proposed some by ourselves and colleagues, some by others working independently and we have today a proliferation of methods which are bewildering to an engineer trying to decide how best to treat his problem. Each of the methods has some foundation in reality, but often the extension beyond the fundamental premise and the mathematical implementation of its underlying concept is quite arbitrary. Adjustable constants are introduced, which can force agreement with experiment for a limited range of the variables but which predict unrealistic behavior in other ranges. It is quite clear that sorting out the relative merits of all the available methods will require not only objectivity but a base of critical experiments carefully designed to show up strengths and shortcomings of each method. Most important is the ability of each method to account for the complexities that enter into the fatigue process. This is a task that still lies ahead for that segment of the engineering community concerned with high temperature fatigue.

It is our hope that this paper will help to clarify some of the problems that still remain to be solved, but also to suggest that good progress is being made.

A BRIEF SUMMARY OF REASONS FOR INTEREST IN HIGH TEMPERATURE METAL FATIGUE

Before discussing the current state of the art with regard to treatment of high temperature metal fatigue it is important to outline at least some of the technologically important applications in which fatigue is of some concern. Following are some applications from my own experience, undoubtedly there are many others.

1. Stationary fossil fuel power generation equipment.
2. Aircraft gas turbines.
3. Reusable rockets.
4. Nuclear power, conventional.
5. Nuclear power, breeder.
6. Fusion equipment.
7. Chemical plants (e.g., coal conversion)
8. Miscellaneous
   a. Die casting dies
   b. Molds for plastics
   c. Polution control

COMPLEXITIES: ENVIRONMENTS, LOADINGS, MATERIAL RESPONSE

It is also important to express at least some of the "complexities" that are generic to high temperature fatigue. Of course, it is not necessary to list aspects pertinent to sub-creep fatigue that are automatically included: hardening and softening, subcell formation, dislocation agglomeration, void formation, Stage I crack growth, crack linking, striation formation, etc. What we are specially concerned with here are the added complexities associated with the higher atomic mobility, and environmental reactivity that attends operation in the creep range of the material -- temperatures of the order of one half or more the melting point. Among the most important of these factors are

1. Environmental interaction
   a. Surface effects
   b. Rapid diffusion
2. Metallurgical instabilities
   a. Defect agglomerations
   b. Phase precipitations
   c. Grain growth, boundary migration
3. Multi-model deformation and fracture mechanisms
   a. Large strain rate effects
   b. Grain boundary sliding
   c. Inter-relation between deformation and fracture
   d. Alternate types of deformation mechanisms (Ashby deformation maps)
4. Broadening relation between stresses and strains
   a. Same deformation at different stresses
   b. New meaning of mean stress effects
5. Healing effects
   a. Reduced damage for some materials by reversing creep in single hysteresis loop
   b. Healing effects by successive hysteresis loop

6. Radiation damage
   a. Lattice disruptions affecting ductility and tensile strength
   b. Special importance in LMFBR and Fusion equipment

SOME ALTERNATIVE FORMS FOR TREATING HIGH TEMPERATURE FATIGUE

Over the last 10 to 15 years a large number of methods have been proposed for treating high temperature fatigue. In each case there is a basic link in the framework of the method to one or more of the mechanisms outlined which is specially relevant to the high temperature problems treated. However other mechanisms are either ignored or treated peripherally. How well each method can handle the overall high temperature picture provides, therefore, a measure of its general merit. But, of course, it should be emphasized that the relative merits of the methods will depend on the pertinence of its underlying principle to the presence of the related factor in the particular material and application. Thus one method may be more pertinent for one set of parameters, another method for a different set of parameters. Several methods developed within the United States are listed below, but space does not permit even a brief summary of their underlying concepts.

1. Time and Cycle Fraction Summation - Robinson, Taira 1952-1962 (refs. 4 and 5)
2. Ten Percent Rule-Manson, Halford, 1964-1969 (refs. 2, 3 and 6)
3. Time and Cycle Fraction Summation Using Cyclic Creep Rupture Data-Manson, Halford, Spera, 1971 (ref. 7)
4. Frequency Modified Life Equation-Coffin, 1969 (ref. 8)
5. Strainrange Partitioning-Manson, Halford, Hirschberg 1971 (ref. 8)
6. Frequency Separation-Coffin, 1976 (ref. 10)
7. Hysteresis Loop Analysis-Ostergren, 1976 (ref. 11)
8. Energy-Based Analysis-Leis, 1977 (ref. 12)
9. Damage Accumulation-Majumdar, Maiya, 1976-1980 (refs. 13 to 15)

In addition there are a number of variants of these methods, as well as independently constituted methods that bear resemblance to those listed above. Notable among them is the work of Chaboche and colleagues in France (ref. 16).

Because space does not permit a complete discussion of these methods, we shall limit further discussion only to Strainrange Partitioning (SRP) to which we have devoted our major attention in recent years.

STRAINRANGE TYPES - SRP METHOD

The SRP method attempts to take cognizance of two types of deformation that can occur in the creep range for some materials. For example, AISI 316 stainless steel is known to be susceptible to grain boundary (g.b.) sliding when held at constant stress at temperatures within the creep range, but such sliding is absent for very rapid rate loading. When g.b. sliding does occur a considerable amount of distortion is accommodated by slip-plane (s.p.) sliding within the grains. The strain that is introduced by g.b. sliding and attendant s.p. sliding we refer to as "creep". On the other hand, if the loading is rapid there is no time for g.b. sliding to occur, and all the strain is absorbed as s.p. sliding much as plasticity occurs at room temperature by only

s.p. sliding without involvement of g.b. sliding. For this reason we call strain introduced by s.p. sliding as "plasticity" even if it occurs at high temperature.

Four different types of strainranges become possible by combining the two types of strains with their occurrence in the tension and compression halves of the loop. If we label P as "plastic" and C as "creep" strain, and adopt the notation that the first letter refers to the tensile part of the loop and the second to the compressive half, then the four permutations of strainrange that are possible become ϵ_{pp}, ϵ_{cc}, ϵ_{cp}, and ϵ_{pc}.

To understand how the different permutations of loading can lead to different micromechanistic effects, we refer first to the idealized figure 1. Here we show an ϵ_{cp} strainrange, where as seen in the hysteresis loop, the tensile strain is achieved by rapidly raising the stress to some value in the vicinity of the yield point and holding stress constant allowing creep deformation to occur along CD. The compression half of the loop is obtained by very rapid loading, creep effect are minimized, and the deformation takes place by plasticity along DEA. Physically we can envision what happens micromechanistically by examining the sketches figures 1(b) to (d). If we idealize the behavior, and hypothesize that "creep" implies g.b. sliding together with slip plane sliding, while plasticity implies only slip plane sliding, then it can be seen that during CD there will be displacement of one grain relative to the other along the grain boundary GH, while the strain reversal DEA will occur along the slip plane EF. After one loop a small notch remains on the surface at an intersection with a grain boundary. Not only is oxidation more probable at the freshly exposed surface but cavitation along the grain boundary weakens it and should make it a preferred site for further oxidation. Additional cycles of this type of loading exacerbate the damage, each cycle adding more monotonic creep strain along the grain boundary and monotonic plasticity along the slip plane. Final fracture, for materials subject to grain boundary sliding, is frequently intercrystalline, and it occurs after relatively few cycles compared to other ways of imposing the same strainrange.

The other types of strainrange ϵ_{pp}, ϵ_{cc} and ϵ_{pc} involve different types of combined slip plane and grain boundary sliding, producing different deformation effects and life relationships. An overall view of the four types of strain range, the idealized associated hysteresis loops, and the manner in which the two types of sliding interact are shown in figure 2. We shall discuss each of these separately, and illustrate typical results obtained for materials amenable to these kinds of strain interactions. An overall view of the differences in micromechanistic events will now be discussed.

PP Strainrange

For PP loading both the tensile and compressive strains are imposed rapidly, allowing no time for creep to occur. As seen in figure 3, only slip plane sliding occurs, very similar to sub-creep behavior. In a large measure the slip that takes place in tension is reversed by the compression strain, but this reversal is not complete. Small intrusions can develop at some of the interactions of the slip planes with the surface, such as shown in the figure. Extrusions may occur in other locations, whereby some planes of metal project forward of the surface. In either case the nascent surfaces are

especially prone to oxidation. Life, then, depends on damage accumulation in the slip planes and on surface notching and oxidation. After sufficient local damage occurs, microcracks initiate and eventually a large crack develops either independently or by merging of several cracks. This "dominant" crack then continues to grow rapidly, aided by the high stress concentration it develops at its front. Crack growth then proceeds according to the laws of fracture mechanics, just as such growth occurs in the sub-creep range. In fact PP loading can be treated according to all procedures developed for sub-creep analysis except that the mechanical properties of the material at the test temperature must be used.

Figure 4 shows an example of PP surface damage for 316 SS at 705° C (1300° F). The slip planes have been decorated by etching and it is clear that there is much slip plane damage even after only 20 percent of life. Surface oxidation sites are evident both in the slip planes and at grain boundaries (which usually are oxidation prone, even in the absence of grain boundary sliding, because of the complex composition and dislocation content of these boundaries). The oxidation is not deep, however, and although oxidation does enhance fatigue failure, it is not the primary cause of failure, slip plane sliding is the culprit, since the cycles take too little time to allow serious oxidation to occur. We shall return to the question of oxidation later.

CC Strainrange

An enlarged view showing completely reversed creep strain, is shown in figure 5. Here we see that grain boundary sliding occurs to and fro as the loading alternates between tension and compression. Such sliding can fracture brittle hard particles serving as nucleii for voids in the grain boundaries. The sliding of several adjacent grains has several effects. Because of the high hydrostatic stresses present at triple-points, some local fracture will occur. These "wedge fractures" act as nucleii for further crack growth. The hydrostatic tensile stresses near the triple points also induce local voids, which can combine with and enlarge the wedge cracks.

Another important source of grain boundary damage is the intersection of slip bands with the grain boundary. While slip plane sliding is not directly implied in the designation CC, there must be induced slip plane sliding as the grains distort to maintain some kind of continuum while the grains slide. If the grains could slide as rigid blocks, they would induce very large wedge cracks, which would very quickly disintegrate the microstructure. But because of the cohesion of grains at triple points, they provide resistance against development of large discontinuties. To prevent total breakdown of continuum, the grains distort by sliding along the grain boundaries. But in CC straining, the only amount of slip plane sliding generated is that due to near-continuum considerations, not the arbitrary amounts involved in any strainrange involving plasticity. Of special importance is that the intersection of a slip plane and a grain boundary provides a region of dislocation pileup. The strain concentration, and the diffusion of dislocations into the grain boundary can therefore become the origin of a void. As will later be discussed, such intersections can become important points of fracture, even for materials which do not allow grain boundary sliding.

Finally, we see in figure 5 that an oxide forms on the surface of a material exposed to oxygen because of the relatively long time involved in generating the creep.

During the compressive creep reversal several events occur as sliding in the opposite direction occurs along the grain boundaries. The wedge cracks get smaller, but are not completely removed. The particles may regain their original geometry, although their interface cannot completely re-weld. Some voids may collapse, although at the intersections of slip planes and grain boundaries there may even develop a proliferation of voids because different slip planes may be effective during compression. In addition we show in figure 5 some indication of grain boundary migration which occurs both during tension and compression as the grain boundaries rotate in attempt to line up along 45° planes to facilitate sliding. As they rotate they leave wakes of voids that were generated in various positions of the grain boundaries. In evaluating the nature of CC straining we can see, therefore, that both grain boundary and slip-plane damage can occur. But neither is severely damaging, because of near-reversal of each type of slip. Figure 6 shows the CC damage incurred at the surface of a 316 SS specimen tested at 1300° F. The surface was etched to decorate the slip planes. It is very clear that both grain boundary and slip plane damage is present. Figure 7 shows a close-up of the cracking of the 316 SS in CC loading. The triple point fracture is clear as are evidence of voids along the boundaries. Because of the competition of both types of damage, fracture surfaces may show patches of both intercrystalline and transcrystalline fractures. Nor is it surprising, therefore, that one investigator reporting on the fatigue of one lot of a material will find it intercrystalline, whereas another investigator reporting on another lot will observe only transgranular failure.

Figure 8 shows an example of grain boundary cracking in CC loading for a nickel-base superalloy MAR-M 200. As shall be explained later this material is not subject to grain boundary sliding but the cracks occurred in the grain boundaries (or interdendritic boundaries) anyway. Probably the crack origins were intersections of slip planes and the boundaries. Because the boundaries are brittle in this material, the local fractures agglomerated to produce a totally intercrystalline failure.

Figure 9 shows an interesting example of grain boundary migration during CC loading for a tantalum alloy T-111. Notice broadening of the grain boundaries close to 45° to the loading axis. These tests were conducted at TRW under NASA contract to evaluate SRP concepts on ultra-high temperature materials under very high vacuum. The grain boundary rotation is decorated by the void left in its wake as it rotates.

PC Strainrange

Here the tension half is plastic flow, compression is creep. Figure 10 shows details of the pertinent phenomena. Tension involves only plasticity, and although no slip bands that intersect a grain boundary are shown in the tension side of figure 10, such intersections can serve as nucleii for voids as much as those shown in the compression side. Voids can thus form along grain boundaries, as in CP, but voids would have a tendency to collapse as they form because of the compressive stress field present during the creeping

half of the cycle. This difference is the major one distinguishing PC and CP from the standpoint of slip plane/grain boundary interaction. Shear fracture voids can also be generated in PC, but unlike in CC, can not heal as readily. It is clear from figure 10 that the consequence of slip plane sliding during tension and grain boundary sliding in compression is the formation of a "tongue" (or a recess if the slip band is below the grain boundary) of metal that overhangs the specimen between the participating slip plane and grain boundary. Figure 11 shows a photomicrograph of such a feature in Udimet 700, a nickel-base superalloy tested at 760° C (1400° F). However, here the tongue is formed by material between slip bands rather than between grain boundary and slip plane.

An important factor that can influence the life in PC loading is oxidation. The role of oxidation for PC differs from that for any of the other types of strainrange because of the special opportunity for a thick adherent oxide to develop during the relatively long, slow compression creep. When the strain is suddenly and rapidly reversed to tension, the oxide cracks. Stress concentrations associated with these cracks can start and propagate fatigue failures in the substrate metal.

Figure 12 shows a striking example of PC cracking in 316 SS. The birch-bark appearance of the cracked oxide is shown in figure 12(a). Even after the oxide was removed, some of the deeper cracks had penetrated into the metal substrate, as seen in figure 12(b). These cracks, thus, are not so much related to grain boundary/slip plane interaction as they are to oxide-induced cracking.

Another example of the role of oxide cracking in starting a substrate crack is shown in figure 13. Here the material is H-13 steel,a tool steel used in dies of die-casting machines. The material is very strong, and has good fatigue characteristics. But its relatively low oxidation resistance causes oxide buildup. It is easily seen in this figure that the deep cracks start from cracks in the oxide.

Under some conditions PC loading can result in grain boundary cracking. A material like the nickel-base superalloy MAR-M 200 is designed to have strong grain boundaries in order to resist creep. The PC loading does not, in fact, cause grain boundary sliding because of the strength of boundaries. However, fractures induced by intersections of slip planes and grain (or interdendritic) boundaries cause local fractures in the brittle boundary. The final fracture results form the joining and extension of these local cracks. Figure 14 shows the cracking of MAR-M 200 in PC loading to be in the boundaries. The contribution of oxidation as a crack starter is also seen, although because of the high chromium content of this alloy it is fairly resistant to oxidation.

CP Strainrange

This type of strainrange, in which creep along grain boundaries occurs in tension, while plasticity occurs along slip planes in compression, has already been discussed in connection with figure 1. Some additional details are shown in figure 15. All the fractures involved have already been discussed in connection with the other strainrange types. However, it is important to

recognize that here as with PC straining we have no "healing" by strain reversal of the same type. So the ratcheting of both creep in one direction and plasticity in the other can be very damaging. The additional source of void formation at the intersection of a slip plane and grain boundary must be included among the mechanisms that make this type of strainrange the most damaging of all for many types of materials. Figure 16 shows how voiding and cracking actually forms in CP loading at such intersections.

Figure 17 shows CP intercrystalline cracking of the tantalum base alloy T-111 in ultra high (10^{-8} torr) vacuum, indicating that grain boundary cracking did not require oxidation. Finally, in figure 18 we show a comparison between the nature of fracture and the number of cycles to fracture for tests of both PC and CP strainrange of approximately the same amplitude (actually the PC strainrange is slightly higher). Exposure time in compression was considerably longer because of the lower creep rate and because the number of cycles withstood was so much higher. Thus, in the PC loading, more oxidation occurred, and of a more detrimental type, than in the CP loading. Also the mean stress for PC loading is tensile while that for CP is compressive. Yet the life for the PC loading was twenty times longer than that for CP. The microstructure for CP fracture is completely intercrystalline while that for PC is transcrystalline. Obviously, for 316 SS the nature of microstructural damage in CP loading is devastating.

LIFE RELATIONSHIPS

Over the past dozen years we have tested many materials using the SRP framework and laboratories in other countries have investigated its usefulness in relation to their problems. In 1978 a NATO AGARD meeting was held in Aalborg, Denmark specifically for the purpose of sharing experiences among the U. S. and European laboratories in the application of this method (ref. 17). While some limitations were recognized, the general usefulness of the approach was verified. More recently the method has been evaluated in Japan, and at least one investigative team (ref. 18) has expressed the conclusion that SRP is ... "the most promising of the methods studied ..." for the types of materials used. Thus the basic concepts behind SRP as both a scientific explanation of material behavior and a technologically viable method have been examined by many investigators. Because of the large variety of interest among them these studies have also led to investigation of numerous materials. As a result we now can classify various nuances of behavior among different classes of materials, and we can catalogue materials according to their characteristic behavior. Such cataloging enables us to understand metallurgical and micromechanistic aspects that would not be possible without broad exposure to at least several types of characteristic response.

Classical Behavior

Because each of the four generic types of strainranges involves different micromechanisms of crack development it would be expected that fatigue lives should differ among them for the same applied strainranges. Many materials do indeed satisfy this expectation. Figure 19(a) shows the life relations for 316 SS. The four Manson-Coffin types of lines are distinctly separated from each other, the PP line being the most benign, the CP the most damaging with a

factor of more than 20 between them. It is interesting that for this material these life relations are nearly independent of temperature (ref. 19) a fact not only of immense practical value but also fundamental significance. The implication is that for this material, life depends only on strainrange, not the stresses required to obtain these strains. Obviously the stresses required to achieve a given strainrange are lower as temperatures are increased.

Figure 19(b) shows the results of another material that behaves in a classic pattern. The iron-base alloy A-286 was tested both in air and at high vacuum at 1000° to 1400° F. Four well-established independent lines were found under each test condition. Lives in vacuum were, of course, higher than in air, indicating the importance of oxidation of this low-alloy steel at such high temperatures. But the displacement among the lines for the generic strainranges are present even in vacuum, indicating that such displacement is fundamental to the type of strainrange, not oxidation.

Universalized Life Relationships

Because so many of the materials we have investigated follow well-behaved life relationships several attempts have been made to develop universalized equations similar to the Universal Slopes Equation (ref. 1) in order to estimate life when actual life lines are not known. An early formulation was made by the senior author in 1972 (ref. 20); however, Halford and Saltsman (ref. 21) have recently based a new set of equations on more extensive data. Their equations are shown in figure 20. Here D_p is the ductility based on reduction of area in an ordinary tensile test, and D_c the ductility in a tensile creep test of approximately the same duration as the fatigue test predicted. These equations agree quite well with the data for many materials and we shall return to them in a later discussion.

Materials with Coincident Life Relations

Some materials do not display any difference in life to the type of strainrange applied. Figure 21 shows the relations for MAR-M 200 wherein all life lines coincide. This material is a highly strengthened nickel-base superalloy, with a composition chosen so as to strengthen the grain boundaries against grain boundary sliding in order to resist creep at the high temperature of its intended use in advanced turbojet engines. It can readily be seen, therefore, why it does not respond to the complex interaction of slip plane and grain boundary sliding. All deformation is in the slip planes, whether time-dependent or time-independent. Such materials do not negate the validity of the SRP approach; the implication only is that the generality of SRP is not needed for such materials, but there is no inconsistancy of behavior with SRP concepts. In fact, it is the process of conducting tests of the SRP generic type that informs us that no grain boundary sliding is involved when all the lines coincide. The role of intersections between slip planes and grain boundaries in developing local grain boundary cracking helps us to understand the type of fractures that already have been discussed in connection with figures 8 and 14.

Materials with Three Coincident and One Displaced Life Line

Some materials such as IN-100 and H-13 steel display PP, CP, and CC as a single life relation, while the PC line is displaced toward lower life. These materials are shown in figure 22. Here the implication is that oxidation is a very important parameter in degrading the PC life relation, as shown in figure 12. Were it not for the special effect of oxidation on the PC life, all the lives would coincide. In other words, such materials do not involve interaction of slip plane and grain boundary sliding, all deformation is due to slip plane sliding. But PC, with its tendency to form heavy oxide scale, which cracks during rapid tensile loading, adds crack starters to the surface, and degrades life.

Maverick Materials

Some materials behave in a manner that seems unexpected at first, but can be better understood in further reflection according to SRP concepts. One such material is IN-792 + Hf. This nickel base superalloy contains a large addition of Hafnium which has the effect of ductilizing it, particularly in creep tests. The SRP life lines are as shown in figure 23. Strangely, and uniquely among all materials we have as yet experienced, the CP and CC strainranges are the least damaging, while the PP and PC are the most damaging. For this material a CP strainrange gives a life 10 times greater than a PP strainrange. The CP tests exhibit mixed intergranular and transgranular fractures while PP tests cracked intergranularly.

To understand this unusual behavior at the phenomenological level we invoke the universalized life relations of figure 20. These relations tell us we must conduct ordinary tensile tests to obtain tensile ductility, thereby estimating the PP and PC life lines. They also tell us that ductilities measured in a creep test should be used for estimating CP and CC lives. Indeed, for this material the creep ductility is greater than the tensile test ductility. Calculations produce the results shown in figure 23 which shows that the life relations should be exactly as they are predicted by the universalized life relationships.

But why should creep ductility be higher than tensile ductility? Annis, VanWanderham and Wallace (ref. 22), in presenting the original SRP data for IN-792 + Hf, point out that specimens tested in CP exhibited the presence of stacking faults -- mismatches in the stacking of crystallographic planes -- that helps to homogenize the deformation and hence enhance the creep ductility. Such stacking faults were not observed in PP tests. It appears that for this material that deformation takes place in slip planes, but for creep, wherein formation of stacking faults permits more diffuse mechanisms of dislocation movement, the strain is dispersed among more slip planes. Thus, with creep ductility higher than tensile ductility the CP and CC strainranges result in longer lives than PP and PC.

As for the intergranular nature of the fracture, despite the non-participation of the grain boundaries, the reason probably lies in the intersection of the slipping planes with the brittle grain boundaries starting many local cracks. Thus, while all the deformation is in the slip bands, these bands can absorb much strain and do not initiate fracture. Instead, the grain

boundary cracks at numerous intersections between slip planes and grain boundaries eventually join to produce intercrystalline failure for all the generic types of SRP strainranges.

Cumulative Fatigue Damage

Up to this point the discussion has related to life relationships for hysteresis loops of pure generic strainrange types. In practice such loops rarely occur. We must consider, then, loops containing more than one strainrange, as well as independent loops which can interact to produce synergistic effects.

Single Loops Containing More Than One Strainrange

Figure 24(a) shows a still-idealized but more realistic loop which contains PP, CC, and CP strainranges. Here the tensile strain consists of 1 percent plasticity and 2 percent creep, while the compressive strain consists of 1 percent creep and 2 percent plasticity. Thus, to interpret this loop in terms of its strainrange components (partitioning of the loop) we regard the PP component to be generated by the tensile plasticity AB' balanced by half the compressive plasticity DE', the CC component to be generated by half the tensile creep B'D balanced by the compressive creep E'A and the CP component to be generated by half the tensile creep B'D balanced by half the compressive plasticity DE'. For simplicity we have, therefore, chosen PP = CC = CP = 1 percent. However, it will be seen that the conclusions to be reached would be valid for any combination of strainrange magnitudes.

Analysis by linear damage rule. - In our early work we regarded a loop such as figure 24(a) to be composed of 3 loops each of 1 percent, but having generic types PP, CC and CP. The implication is shown in figure 24(b), where the three independent 1 percent strainrange loops are drawn. When life analysis was applied, we reasoned that in one loop of ABCDEF would use up $1/N_f$ of life. Since one loop of the PP, CC and CP, each of 1 percent, the life used up by applying the three generic loops would be

$$1/N_{pp} + 1/N_{cc} + 1/N_{cp}$$

where N_{pp} is life on the PP curve for 1 percent strainrange, and with similar definitions for N_{cc} and N_{cp}. Thus we developed the Linear Damage Rule

$$1/N_f = 1/N_{pp} + 1/N_{cc} + 1/N_{cp} \qquad (1)$$

This equation was satisfactory for materials life 316 SS, for which four independent life relations applied, and which were our main preoccupation in the early work.

As we started to consider materials of other character, a dilemma arose in regard to the use of the Linear Damage Rule. Consider, for example, a material (like MAR-M 200) for which all the life lines are coincident. Figure 25 shows an idealized curve. The calculation for such a material is also shown in figure 25. Applying the Linear Damage Rule using

$$\varepsilon_{pp} = \varepsilon_{cc} = \varepsilon_{cp} = 1 \text{ percent}$$

the life components of the 1 percent strainranges are each 10 000 cycles, and the calculated life becomes

$$10\ 000/3 = 3\ 333 \text{ cycles}$$

However, since all types of strainranges produce the same life at the same strainrange, there is no reason to assume that a 3 percent strainrange should not be the same as any other strainrange of 3 percent, which is 1000 cycles according to the figure and not the 3 333 value just calculated. Thus there is considerable discrepancy between calculations by the Linear Damage Rule and reasonable expectations. It was considerations such as this that led to the development of the Interaction Damage Rule.

The interaction damage rule. - In devising an alternate damage rule for combining the effects of concurrent strainranges we reasoned that the life relations as we determine them are valid ony for loops containing the single generic strainrange involved. When two or more strainranges are present, these life relations must be modified -- in other words there is an "interaction" among the concurrent strainranges which influences all the life curves. By fortuitous choice of the analytical function governing the interaction we arrived at what we called the "Interaction Damage Rule." Thus, life calculation became according to the relation

$$1/N_f = f_{pp}/N'_{pp} + f_{cc}/N'_{cc} + f_{cp}/N'_{cp} \qquad (2)$$

where $F_{pp} = \varepsilon_{pp}/\varepsilon_{in}$, $f_{cc} = \varepsilon_{cc}/\varepsilon_{in}$, and $f_{cp} = \varepsilon_{cp}/\varepsilon_{in}$. This formulation changes the N_{pp}, N_{cc}, and N_{cp} values of equation (1) to N'_{pp}, N'_{cc}, and N'_{cp} which are the life values from the generic life relations at the total strainrange of the original hysteresis loop. In this case, then

$$N_{pp} = N_{cc} = N_{cp} = 1000.$$

Since

$$f_{pp} = f_{cc} = f_{cp} = 1/3,$$

the calculated value of N_f also becomes 1000, as would be expected. Thus the Interaction Damage Rule does not suffer from the same problem as does the Linear Damage Rule for cases such as this one. Nor have we found any situation in which it gives unreasonable results.

A new interpretation of the interaction damage rule. - For more than a decade we attempted no interpretation of the Interaction Damage Rule other than its apparent usefulness in computing life once the hysteresis loop was partitioned into its generic strainranges. Recently, however, during an attempt to apply it to synthesis of independent loops, a new interpretation arose which has been helpful not only for this intended purpose, but actually provided insight into the physical meaning of the rule.

Consider equation (2). One way of interpreting it is in the same context as shown in figure 24 for the Linear Damage Rule. In essence it would state that one original hysteresis loop of the three strainrange content is equal to

1/3 loop each of a pure PC and CC and CP, all having the same strainrange as the original loop. Since it is awkward to deal with fractional hysteresis loops we can cross-multiply by 3 to find that three original loops is equal to one each of PP, CC, and CP, all loops of the same strainrange. While we can carry the argument in this way, it is more desirable, as will later become evident, to multiply both sides of the equation by 9, as shown in figure 26. Thus the Interaction Damage Rule implies an equivalence of 9 original loops to the sum of three each of the generic loops on the right side of figure 26. If we attempt, however, to overlay such loops upon each other there is no evident geometric congruence.

Upon further contemplation there does seem to develop a viewpoint that can result in essential geometric coincidence. We make use of the fact that neither the SRP framework nor the Interaction Damage Rule calculation makes any requirement regarding the order of application of the strainranges nor the stresses at which the creep strain is induced. The only requirement, in identifying the problem being used as an example, is that the tension portion of the loop contain 2 percent creep and 1 percent plasticity, while the compression portion contain 1 percent creep and 2 percent plasticity. This requirement fulfilled, SRP would regard the loops to be equally damaging, and the Interaction Damage Rule would calculate the same life. Now there are an infinite number of ways to compound a loop which satisfies this requirement. However, if we add the requirement that both the creep and plasticity be introduced only in lumps of 1 percent, it turns out that there are only 9 ways to draw such loops.

In figure 27 we show these nine ways in tablular form. Along any row the tensile half of the loop is kept the same, while along any column the compressive half of the loop is kept the same. For example, the tension half can introduce the 3 percent in the order 1 percent plasticity/2 percent creep; or it can be 2 percent creep/1 percent plasticity; or 1 percent creep/1 percent plasticity/1 percent creep. Similarly, the compressive half allows three permutations of order. Together, then, there are 9 independent ways to draw loops that satisfy the strain range requirements, and therefore have identical lives according to SRP and the Interaction Damage Rule.

Now if we superimpose the nine equally damaging hysteresis loops, they indeed trace out exactly three each of the independent generic strainrange loops required by figure 26. This can easily be seen by using transparent overlays, but the easiest proof is to determine which elements are traced out by the two alternative constructions. Figure 28 shows the results of such a tally. Each segment of loop traced out is identified on the overlay, and how it is traced out by combining the nine equivalent original loops, or by the three generic loops, is shown in the table. It is clear that, segment for segment, both sequences trace out <u>exactly</u> the elements. Only the linear elastic lines, traced out as stress changes occur, are not duplicated. These lines presumably cause no damage because no inelastic strain is involved. (Actually the whole construction is idealized; actual paths should differ to some extent because of oxidation and metallurgical changes associated with various time effects. But consideration of these complexities opens whole new fields of investigation. See ref. 23 for fuller discussion.)

To put these results into a useful perspective, we can postulate a principle of <u>equivalent miromechanistic damage</u>: "Two loading histories produce

the same micromechanistic damage if they trace out identical hysteresis paths, element for element, although the sequence of introducing the elements may vary within tne two histories." On this basis we can interpret the Interaction Damage Rule as determining the average damage induced among a number of paths which, presumably consistent with the SRP principle that only strainrange content governs damage, have the same damage. For the problem illustrated the Interaction Damage Rule averages the damage for all combinations of loops that introduce the creep and plasticity in quantum lumps, although many other combinations exist. In this way the Interaction Damage Rule teaches us how to determine the damage of a loop combining two or more strainranges from loops that contain only generic strainranges. Since life values for the latter type of loops are fundamental data usually available, study of the damage of more complex loops becomes tractable.

Use of Interaction Damage Rule to Synthesize Loops--"Healing"

Having indicated that the reinterpretation of the Interaction Damage Rule arose out of our interest in its application to loop synthesis, particularily how "healing" can take place when sequential CP and PC loadings occur, let us now describe this use. For brevity we shall just demonstrate the principle and show some limited experimental results. More complete details are contained in reference 23.

Consider a simple case in which a CP loop is first applied to a material, and later a PC loop is applied. Is it possible that the material will perceive the compressive creep of the PC loop to reverse the tensile creep of the CP loop, thereby "healing" the material in the same sense that a CC loop is less damaging than a CP loop? Figure 29 shows how we are approaching this problem.

The figure shows that at one point in its history the CP loop ABC is imposed at a later time than the PC loop DEF is imposed. We first superpose the two loops in a manner which will make the "healing loop" recognizable, such as shown in the figure. (Of course, this construction alters mean strain, but generally the effect is small. If significant we shall study the effect later.) As seen, then, the combined effect is a CC loop AGFD with strainrange equal to the smaller of the two strainranges (here PC), and a loop CEGB which contains both PP and CP components, and has a total strainrange equal to the larger of the two loops. Here ε_1 and ε_s refer to the inelastic strainranges of the intial large CP loop and small PC loop, respectively. Partitioning CEGB into its PP and CP components, it is clear that

$$f_{pp} = \varepsilon_s/\varepsilon_1 \quad \text{while} \quad f_{cp} = (\varepsilon_1 - \varepsilon_s)/\varepsilon_1$$

Thus loop CEGB consists of a fraction f_{pp} of a PP loop of strainrange ε_1 and a fraction f_{cp} of a CP loop of the same strainrange.

Now the CC and fractional PP loop so generated represent completed behaviors which can no longer produce interaction with subsequent loops. But the fractional CP loop can interact with later encountered PC loops according to the same formulation as shown here. It turns out the combined effect of all of these loops does indeed reflect a "healing" by conversion of part of the damaging CP loop into a CC loop.

We can treat more complex loops by the same basic procedure. In the most general case we can combine an arbitrary number of complex loops containing arbitrary strainranges, say rich in CP content, with any specified number of general loops rich in PC content. Damage and healing effects can then be calculated. Details are omitted here, but can be found in reference 23.

Some experience on "healing". - We have conducted only a few experiments to check the validity of viewpoint here expressed. So far the results have been encouraging, but our intent is to do considerable additional testing in the future.

The first set of experiments were carried out by Richard Wesling, a graduate student at Case Western Reserve in 1978. The results are shown in figure 30, and were previously reported by the senior author (ref. 24). Basically many combinations of CP and PC loops of equal strainrange were applied to 316 SS. In some cases the loops were alternated one after the other, in other cases groups of CP loops were alternated with groups of PC loops, and finally large blocks of either CP or PC loops were first applied, followed by a block of the other type of strainrange until failure occurred. In all cases the expected amount of "healing" effect (SRC, Strain Range Conversion) of the combination of strains compared to the damage that would have been expected if the individual damaging effects of the applied loops were simply summed without regard for interaction effects, i.e., by the CF (Cycle Fraction) procedure. These results are shown in figure 31.

A second set of experiments was carried out by another Case Western Reserve graduate student in 1982. Donald Roulett combined CP-rich loops with PC-rich loops of half the strainrange amplitude. In one set of tests these loops were simply alternated, in the other two loops of the PC type strainrange was alternated with a single loop of the CP-type strainrange. The results are shown in figure 32 as bar graphs. Calculations by the theory outlined here, predicted results that were generally 50 to 100 percent higher than calculations based on the independent effects of the loops. The experimental results corroborated the calculations based on interaction healing.

Interaction of high cycle and low cycle fatigue. - The concepts that we have discussed thus far relate to the cumulative damage effects of loops involving strainranges and frequency of application that are of the same order of magnitude, differing by a factor of 10 at most. There are practical cases where the superposed high cycle fatigue and low cycle fatigue involve large differences in amplitude and frequency. A recent case of interest to us is the space shuttle application. Here the main engine components are subjected to infrequent thermal cycles (essentially strainranges of PC type) together with very high frequency low amplitude vibrations (of PP type). To analyze such situations we have applied two recently developed approaches -- the Double Linear Damage Rule, and the Damage Curve Approach (ref. 25). These types of analysis shows that a few cycles of LCF is extremely damaging to the material when interpreted in the context of supporting concurrent or subsequent HCF loading. Figure 33 shows some of the results we have obtained (ref. 26) when interacting these two types of loadings on 316 SS at 705° C (1300° F). Here we have plotted the cycle ratio of the HCF permissible after a specified cycle ratio of LCF has been applied. The curve shows the results of calculations based on the Damage Curve Approach (with similar results obtained for the Double Linear Damage Rule calculations), the data verify these

predictions. We intend to conduct many such tests to verify other predictions, and hopefully at a later date to unify the concepts we have described here in connection with SRP interactions with the rather independent concepts associated with the Damage Curve and Double Linear Damage Rule approaches.

Constitutive Modeling of Compression and Tension Creep Deformation

We shall complete our manuscript with brief reference to a recent study we have conducted to compare creep deformation rates in tension and compression.

Our interest in the special behavior of compressive creep started about 15 years ago when we first conducted cyclic creep tests in an effort to improve the time-and-cycle fraction method of creep-fatigue analyses (ref. 7). Figure 34 shows how these tests were conducted, and some of the results that intrigued us. Stress was alternated at equal values in tension and compression, and maintained in each case until a creep strain of 1 percent was reached. (It was essentially a CC strainrange test, but SRP terminology had not yet been devised.) In any two successive cycles the time to achieve the compressive creep was about 3 times as long as that needed for the tensile creep. Furthermore, both tension and compression times decreased rapidly from cycle to cycle. Obviously some type of metallurgical effect was taking place to soften the material in successive cycles, but of special interest was the difference in creep rate between tension and compression in adjacent loadings where the metallurgy was essentially the same.

Recently, in pursuing our interests in connection with constitutive modeling of cyclic loading, we recalled this peculiar behavior and ran additional tests to determine if creep rate in compression and tension for materials of essentially the same metallurgical state would display this large difference. If so, there was an important implication in regard to constitutive modeling of cyclic strain. The common assumption is that there is little difference between the two, except perhaps for small effects rising out of cross-sectional area changes during the creep. We conducted tests on essentially virgin material and material which had undergone various complex loading histories, including thermomechanical loading in which temperature and strain were simultaneously varied. The results were quite conclusive; specimens of 316 SS in the same metallurgical state always displayed a lower creep rate in compression than in tension at the same magnitude of stress. Figure 35 shows the results for one of the tests. The creep rate in tension was about 5 times greater than in compression. Other types of tests were also conducted (ref. 27).

We also speculated on mechanistic factors that could cause such results. Possibly it is associated with the mechanism of grain-boundary sliding. An analogy was made to friction of a mass sliding on a horizontal surface. If a force is applied to lift the mass upward away from the surface (tension), friction force is reduced. Added pressure (compression) increases the friction force. Alternatively, the effect could be related to imperfections generated in the grain boundaries, such as voids or small cracks. Tension would separate the surfaces in the flawed areas, compression would force them together. Details can be found in reference 27, but the conclusion is incontrovertible that, at least for 316 SS, there was a large difference in

creep rate between tension and compression. What the effect would be for materials like MAR M-200, H-13, or IN-792 + Hf, wherein no grain boundary participation occurs during creep should prove interesting for future research. For those pondering constitutive modeling procedures this observation may provide an interesting challenge to insure that the proper tension/compression characteristics are incorporated in the modeling.

CONCLUDING REMARKS

The recent developments leading to a better understanding of the complex factors that govern high temperature fatigue in some alloy systems stimulate a challenge to expand the knowledge we have already gained and to study other materials in order to learn which phenomena are general and which specific to each system. Considering the immense importance of the subject we can only express the hope that this challenge will be vigorously accepted by many organizations who have a stake in the promise it offers.

REFERENCES

1. Manson, S. S.: Fatigue: A Complex Subject - Some Simple Approximations. Exp. Mech., vol. 5, no. 7, July 1965, pp. 193-226.

2. Manson, S. S.: Interface Between Fatigue, Creep, and Fracture. Int. J. Fract. Mech., vol. 2, no. 1, Mar. 1966, pp. 327-63.

3. Manson, S. S.; and Halford, G. R.: A Method for Estimating High-Temperature Low-Cycle Fatigue Behavior of Materials. Proceedings of International Conference on Thermal and High-Strain Fatigue, The Metals and Metallurgy Trust (London), 1967, pp. 154-70.

4. Robinson, E. L.: Effect of Temperature Variation on the Long-Time Strength of Steels. Trans. ASME, vol. 74, no. 5, July 1952, pp. 777-80, disc. pp. 780-81.

5. Taira, S.: Lifetime of Structures Subjected to Varying Load and Temperature. Creep in Structures, N. J. Hoff, ed., Springer Verlag (Berlin), 1962, pp. 96-119, disc, pp. 119-124.

6. Halford, G. R.; and Manson, S. S.: Application of a Method of Estimating High-Temperature Low-Cycle Fatigue Behavior of Materials. Trans. ASM, vol. 61, no. 1, 1968, pp. 94-102.

7. Manson, S. S.; Halford, G. R.; and Spera, D. A.: The Role of Creep in High Temperature Low Cycle Fatigue. Advances in Creep Design, A. I. Smith and A. M. Nicholson, eds., Halsted Press, 1971, pp. 229-249.

8. Coffin, L. F., Jr.: The Effect of Frequency on High-Temperature, Low-Cycle Fatigue. Proceedings of the Air Force Conference on Fatigue and Fracture of Aircraft Structures and Materials, AFFDL-TR-70-144, 1971, pp. 301-309.

9. Manson, S. S.; Halford, G. R.; and Hirschberg, M. H.: Creep-Fatigue Analysis by Strainrange Partitioning. Design for Elevated Temperature Environment, S. Y. Zamrik, ed. ASME, pp. 12-24, disc. pp. 25-28, 1971.

10. Coffin, L. F.: The Concept of Frequency Separation in Life Prediction for Time-Dependent Fatigue. Symposium on Creep-Fatigue Interaction. R. M. Curran, ed., MPC Publication No. 3, ASME, 1976, pp. 349-363.

11. Ostergren, W. J.: A Damage Function and Associated Failure Equations for Predicting Hold Time and Frequency Effects in Elevated Temperature Low Cycle Fatigue. J. Testing and Evaluation, vol. 4, no. 5, Sept. 1976, pp. 327-339.

12. Leis, B. N.: An Energy-Based Fatigue and Creep-Fatigue Damage Parameter. J. Pressure Vessel Technology, vol. 99, no. 4, Nov. 1977, pp. 524-533.

13. Majumdar, S.; and Maiya, P. S.: A Unified and Mechanistic Approach to Creep-Fatigue Damage. Second International Conference of Mechanical Behavior of Materials, American Soc. Metals, 1976. Also Argonne National Laboratory Report ANL-76-58 (1976).

14. Majumdar, S.; and Maiya, P. S.: Creep-Fatigue Interactions in an Austenitic Stainless Steel, Can. Metall., vol. 18, no. 1, 1979, pp. 57-64.

15. Majumdar, S.; and Maiya, P. S.: A Mechanistic Model for Time-dependent Fatigue. J. Eng. Mater. Technol., vol. 102, no. 1, Jan. 1980, pp. 159-167.

16. Chaboche, J. L.: Continuous Damage Mechanics. A Tool to Describe Phenomena Before Crack Initiation. Nucl. Eng., vol. 64, 1981, pp. 233-247.

17. Characterization of Low Cycle High Temperature Fatigue by the Strainrange Partitioning Method, 46th Meeting of the AGARD Structures and Materials Panel, Aalbord, Denmark. AGARD-CP-243, 1978.

18. Hirakawa, K.; and Tokimasa, K.: Creep-Fatigue Properties of Materials for High Temperature Service. The Sumitomo Search No. 26, Nov. 1981, pp. 118-135.

19. Halford, G. R.; Hirschberg, M. H.; and Manson, S. S.: Temperature Effects on the Strainrange Partitioning Approach for Creep-Fatigue Analysis. Fatigue at Elevated Temperatures, ASTM STP-520, 1973, pp. 658-667.

20. Manson, S. S.: The Challenge to Unify Treatment of High Temperature Metal Fatigue -- A Partisan Proposal Based on Strainrange Partitioning. Fatigue at Elevated Temperatures, ASTM STP 520, 1973, pp. 744-782.

21. Halford, G. R.; Saltsman, J. F.; and Hirschberg, M. H.: Ductility Normalized-Strainrange Partitioning Life Relations for Creep-Fatigue Life Prediction. Environmental Degradation of Engineering Materials, M. R. Louthan, Jr. and R. P. McNitt, eds., Virginia Polytechnic Institute and State University, Blackburg, Virginia, 1977, pp. 599-612.

22. Annis, C. G.; Van Wanderham, M. C.; and Wallace, R. M.: Strainrange Partitioning Behavior of an Automotive Turbine Alloy. (FR-7424, Pratt and Whitney Aircraft; NASA Contract NAS3-18930.) NASA CR-134974, 1976.

23. Manson, S. S.: The Strainrange Conversion Principle for Treating Cumulative Fatigue Damage in the Creep Range. Random Fatigue Life Prediction. (PVP-Vol. 72). American Soc. Mech. Eng., 1983, pp. 1-29.

24. Manson, S. S.: Some Useful Concepts for the Designer in Treating Cumulative Fatigue Damage at Elevated Temperatures. Mechanical Behavior of Materials, Proceedings of the Third International Conference, Cambridge, England, Vol. 1, K. J. Miller and R. F. Smith, eds., Pergamon Press (Oxford), 1980, pp. 13-45.

25. Manson, S. S.; and Halford, G. R.: Practical Implementation of the Double Linear Damage Rule and Damage Curve Approach for Treating Cumulative Fatigue Damage. Int. J. Frac., vol. 17, 1981, pp. 169-192.

26. Manson, S. S.; Halford, G. R.; and Oldrieve, R. E.: Relation of Cyclic Loading Pattern to Microstructural Fracture in Creep-Fatigue, NASA TM-83473, 1983.

27. Manson, S. S.; Muralidharan, U.; and Halford, G. R.: Tensile and Compressive Constitutive Response of 316 Stainless Steel at Elevated Temperatures, NASA TM-83506, 198.

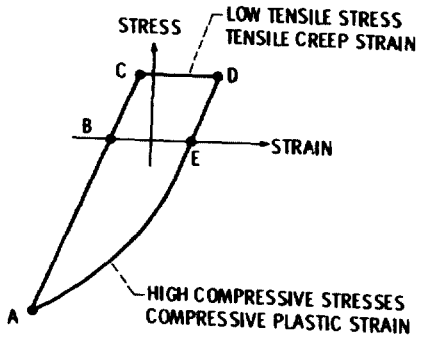

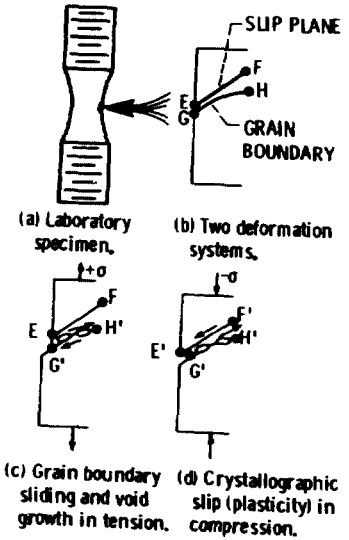

Figure 1. - Schematic illustration of the creep-fatigue interaction occurring when tensile creep occurring along grain boundaries is reversed by compressive plasticity occurring along crystallographic slip planes.

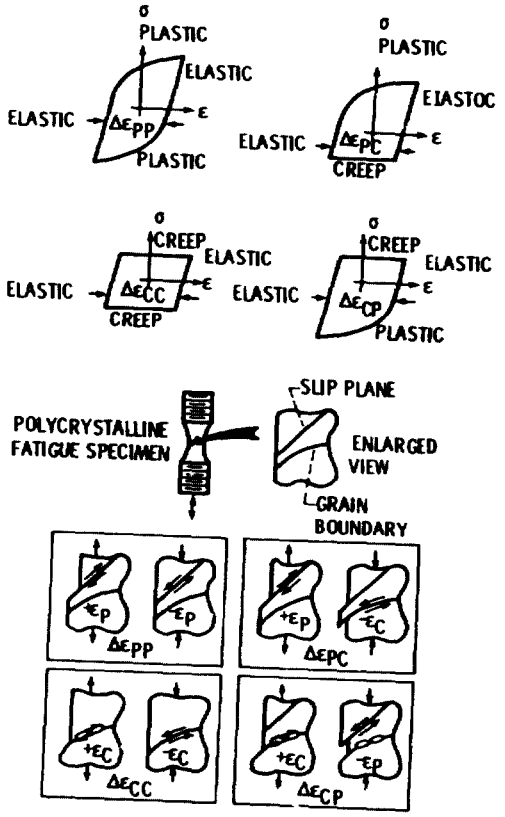

Figure 2. - Simple cyclic deformation models for strain-range partitioning.

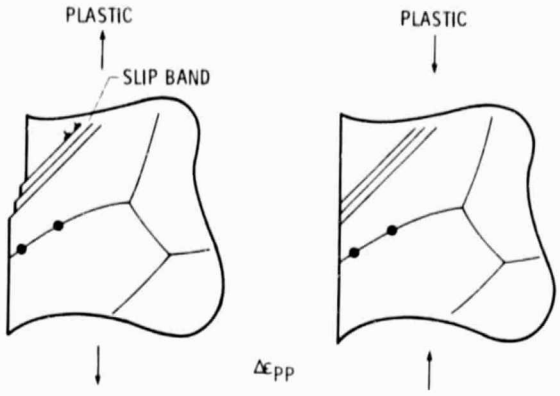

Figure 3. - Schematic illustration of deformation in a PP type of loading cycle.

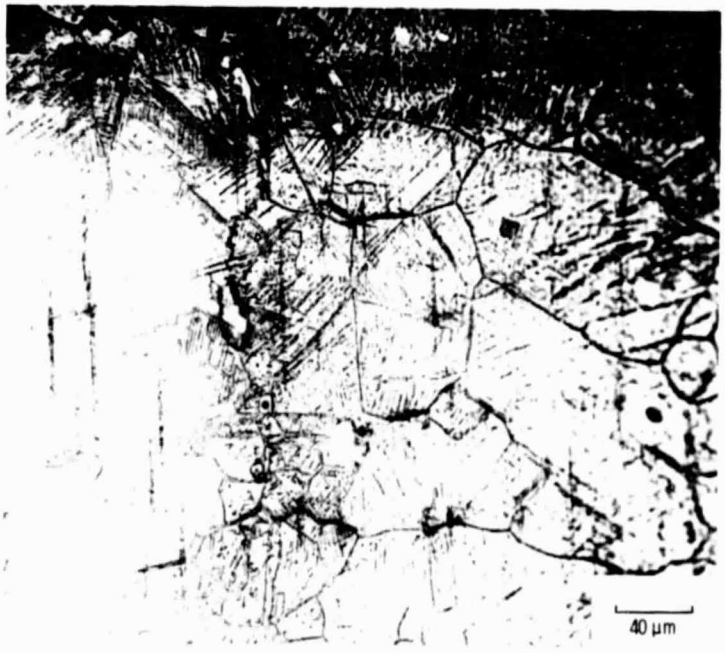

Figure 4. - Example of PP surface cracking 316 SS, 1300^{0}F, 20% N_F.

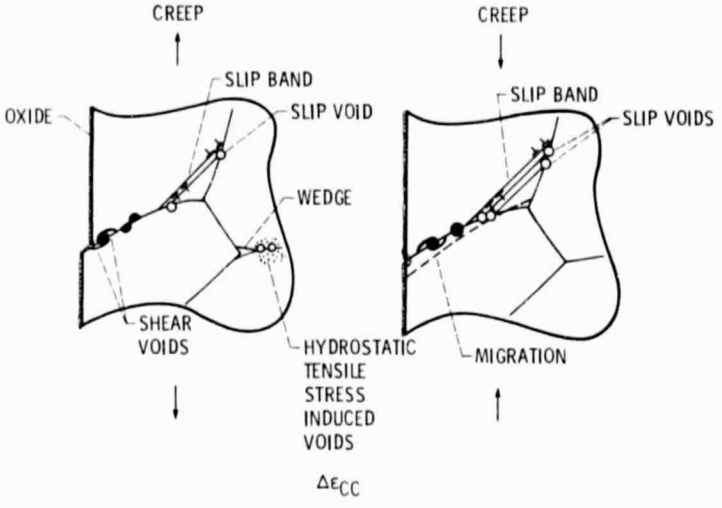

Figure 5. - Schematic illustration of deformation and local fracturing in a CC type of loading cycle.

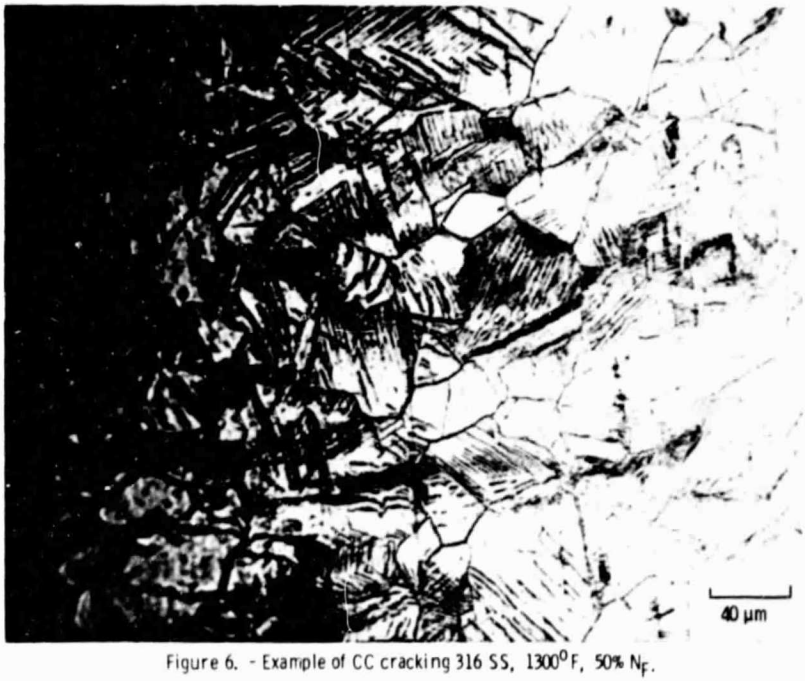

Figure 6. - Example of CC cracking 316 SS, 1300^{0}F, 50% N_F.

Figure 8. - Intercrystalline fracture of Mar M 200, in CC type of loading at 1700°F.

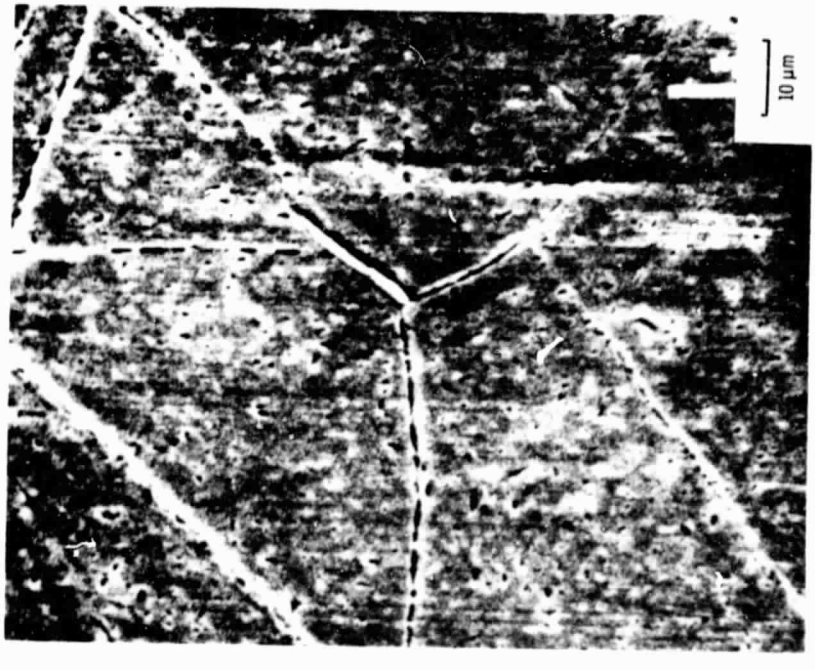

Figure 7. - Enlarged view of CC cracking 316 SS, 1300°F, 50% N_F.

Figure 9. - Grain boundary migration for Tantalum alloy T-111 in high vacuum in CC type of loading cycle.

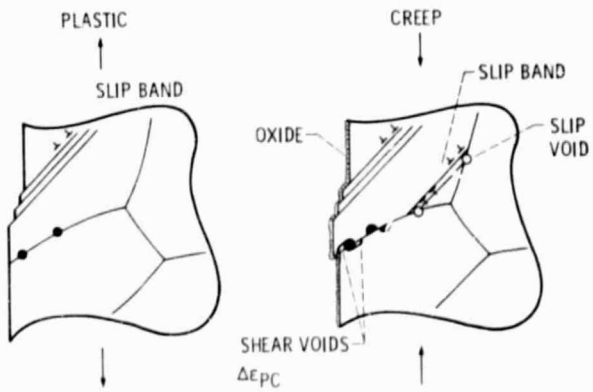

Figure 10. - Schematic illustration of deformation in a PC type of loading cycle.

Figure 11. - Tongue on Udimet 700 at 1400°F in PC type of loading.

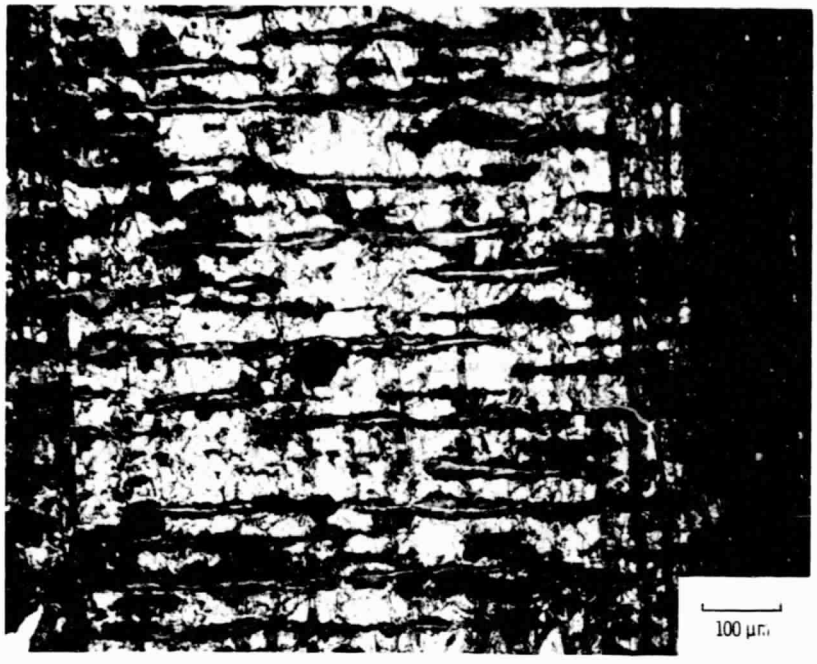

(a) Before oxide removal.

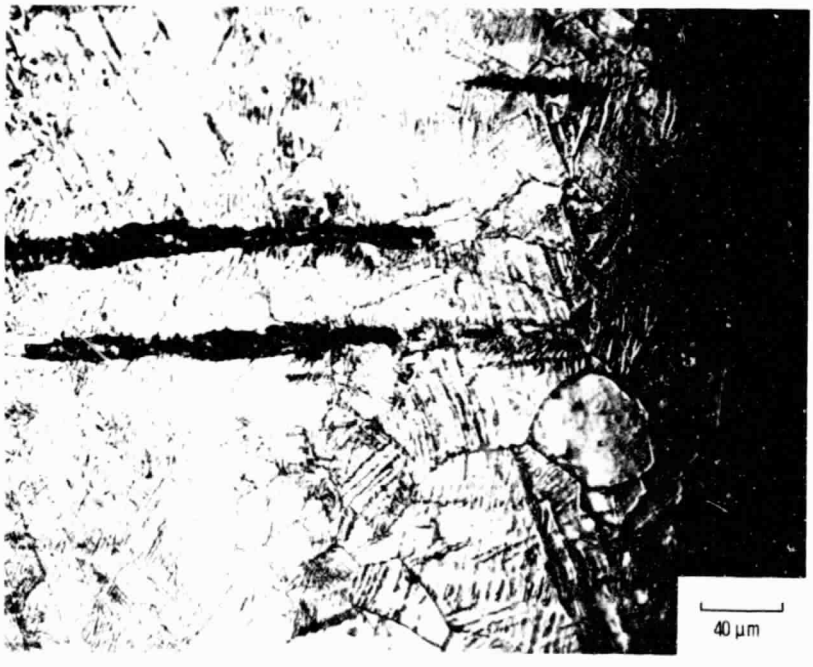

(b) After oxide removal.

Figure 12. - Examples of PC fracture initiated by oxide cracking in 316 SS at 1300^{0}F.

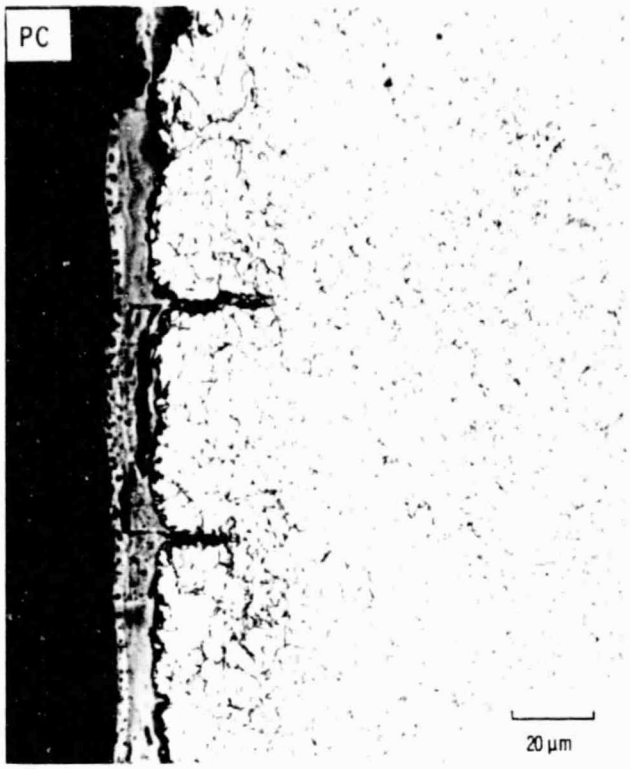

Figure 13. - Creep-fatigue cracking of H-13 tool steel at 1100°F under PC type of loading.

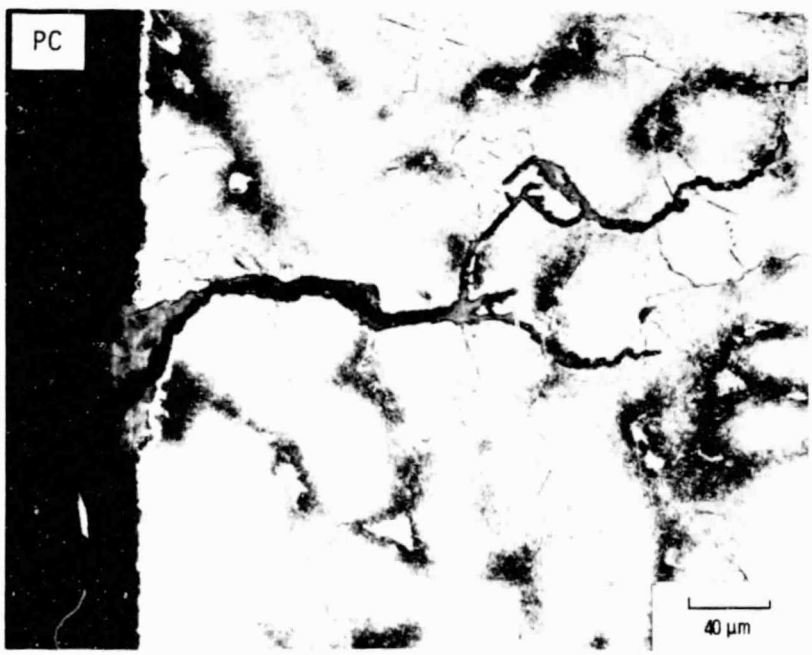

Figure 14. - Example of PC cracking in Mar M-200 at 1700°F.

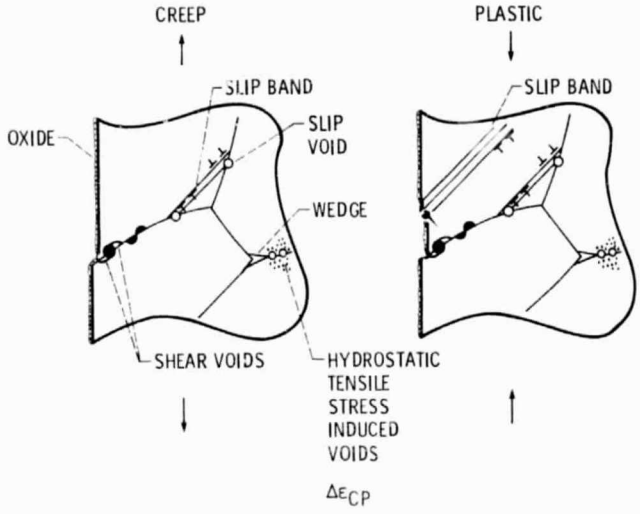

Figure 15. - Schematic illustration of deformation in a CP type of loading cycle.

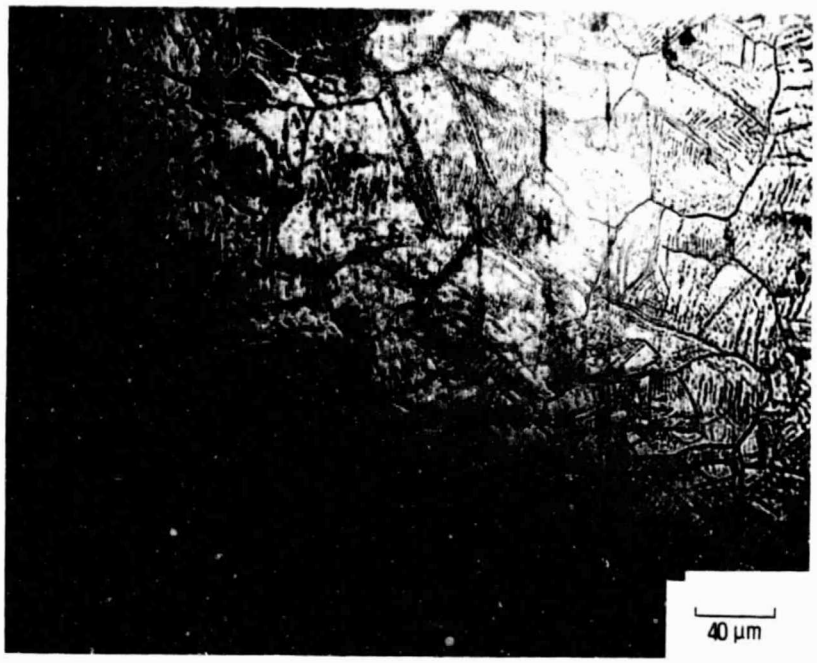

316 S.S. 1300°F, 10% N_F.

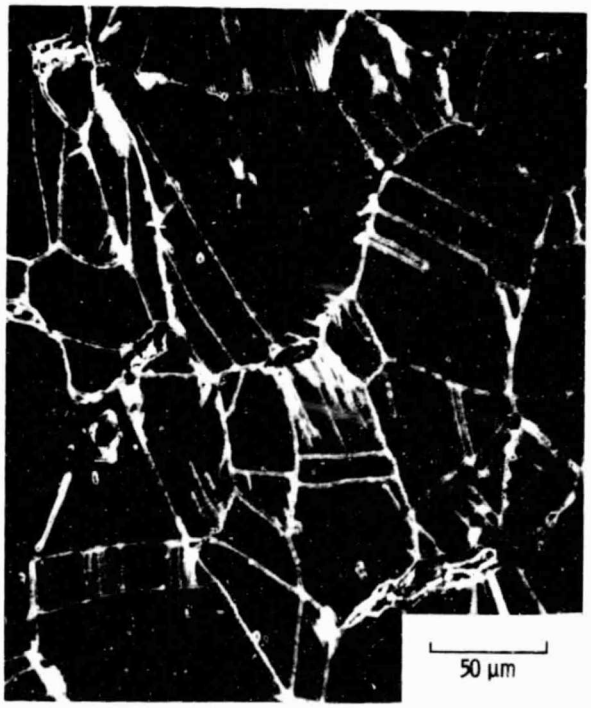

Figure 16. - Examples of CP cracking in 316 S.S. at 1300°F.

Figure 17. - Example of CP cracking in Tantalum alloy T-111 in high vacuum.

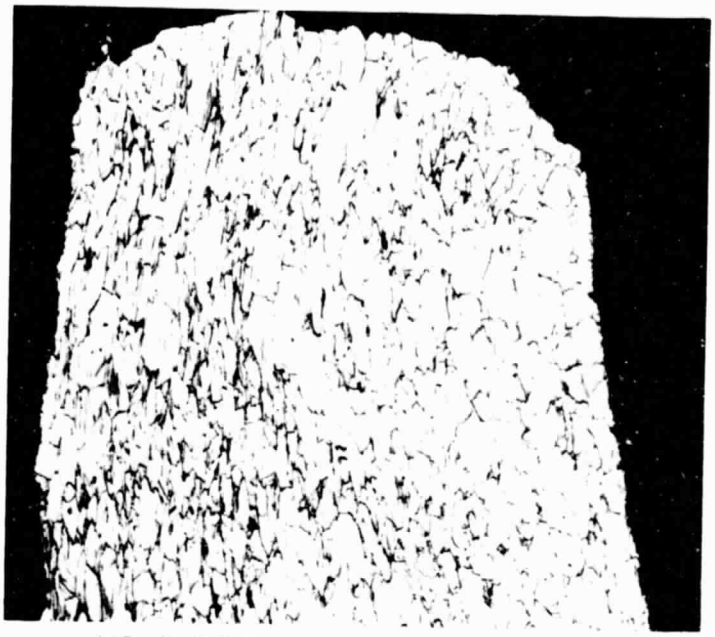

(a) Tensile plastic flow, compressive creep. $\Delta\epsilon_{pc} = 0.0162$, N = 264.

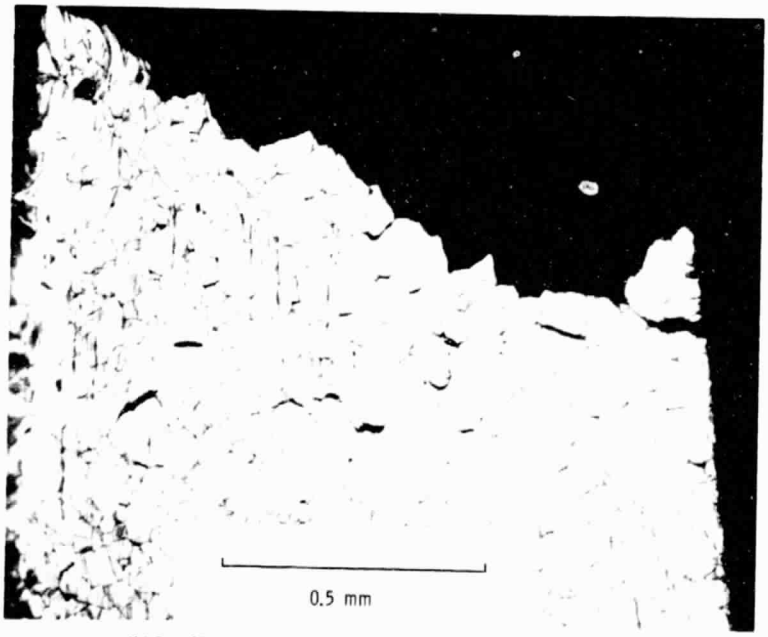

(b) Tensile creep, compressive plastic flow. $\Delta\epsilon_{cp} = 0.0147$, N = 15.

Figure 18. - Failures in 316 SS at approximately equal strainranges, (a) PC, (b) CP.

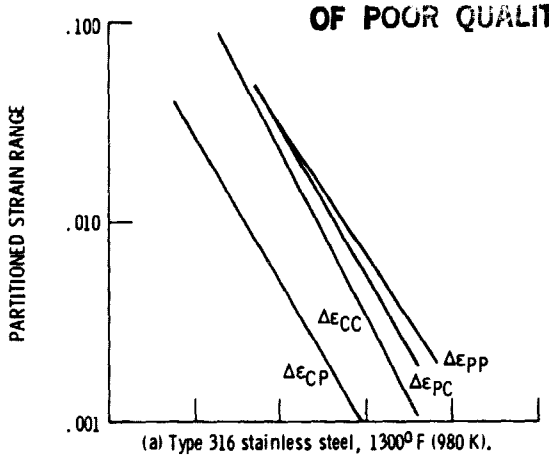

(a) Type 316 stainless steel, 1300° F (980 K).

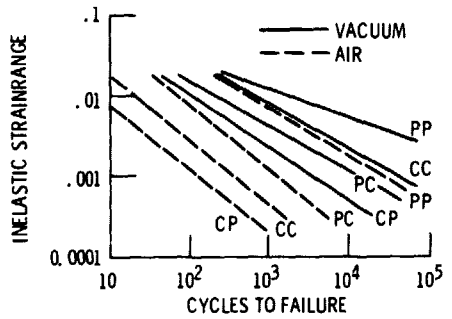

(b) Effect of environment on relations for strainrange partitioning of A-286, 1000 - 1400° F.

Figure 19. - Summary of partitioned strain range-life relations.

$$\Delta\varepsilon_{PP} = 0.50\, D_P\, (N_{PP})^{-0.60}$$

$$\Delta\varepsilon_{PC} = 0.25\, D_p\, (N_{PC})^{-0.60}$$

$$\Delta\varepsilon_{CC} = 0.25\, (D_C)^{0.60} (N_{CC})^{-0.60}$$

$$\Delta\varepsilon_{CP} = 0.20\, (D_C)^{0.60} (N_{CP})^{-0.60} \text{ (TRANSCRYSTALLINE)}$$

$$\text{OR } \Delta\varepsilon_{CP} = 0.10 (D_C)^{0.60} (N_{CP})^{-0.60} \text{ (INTERCRYSTALLINE)}$$

Figure 20. - Universalized strainrange partitioning relations.

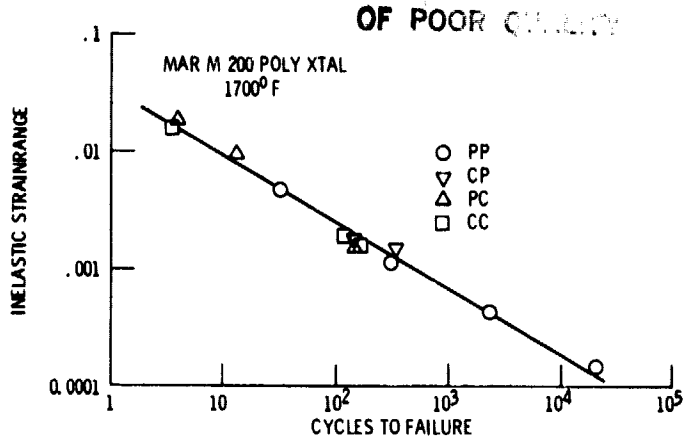

Figure 21. - MAR M 200 SRP life relations.

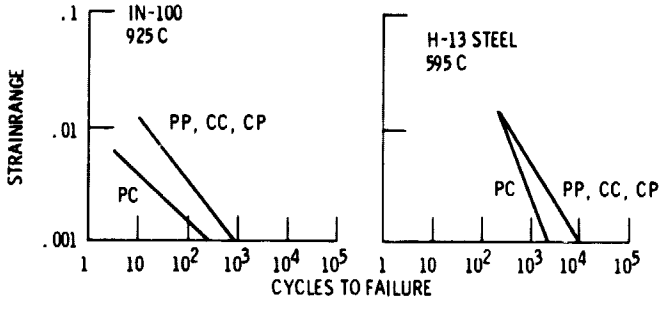

Figure 22. - SRP life relations for IN 100 at 925° C and H-13 tool steel at 595° C.

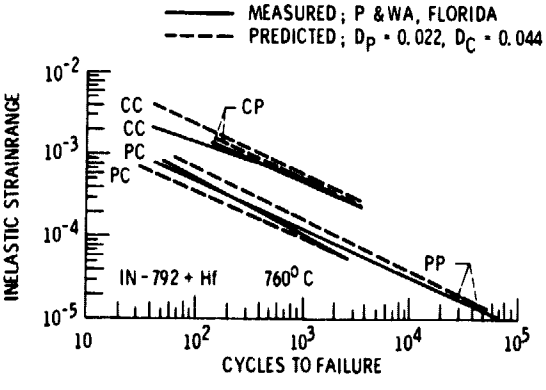

Figure 23. - SRP life relations for IN 792 + Hf at 760° C.

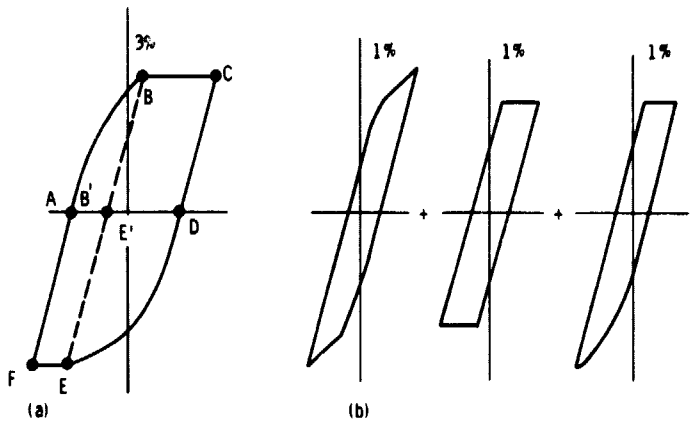

Figure 24. - Analysis of complex loop by linear damage rule.

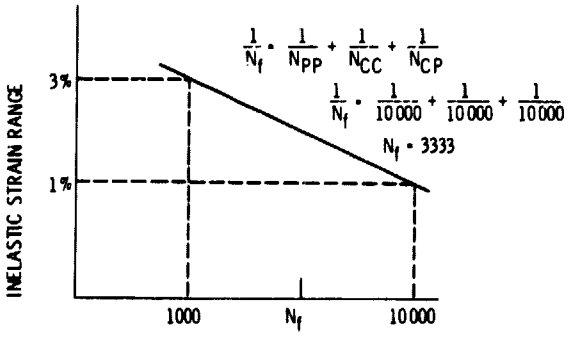

Figure 25. - Analysis by linear damage rule for material with idealized single life relationship.

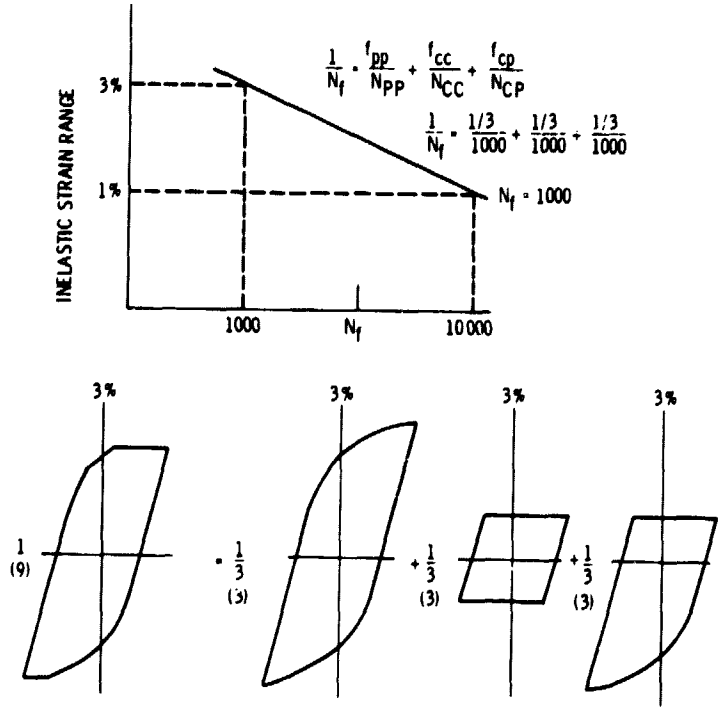

Figure 26. - Hysteresis loop summation by the interaction damage rule.

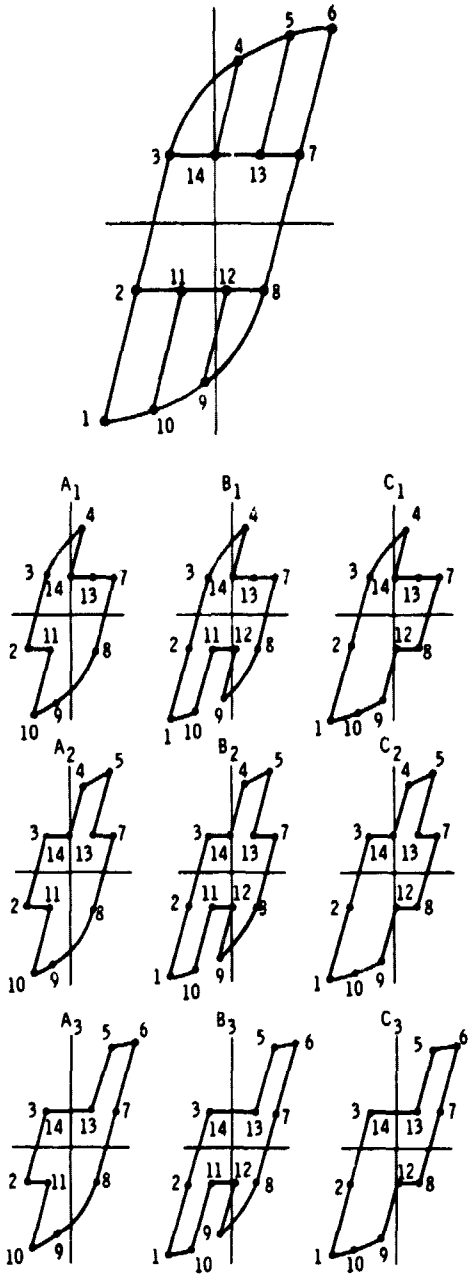

Figure 27. - Nine different hysteresis loops with same PP, CC, CP components of strain.

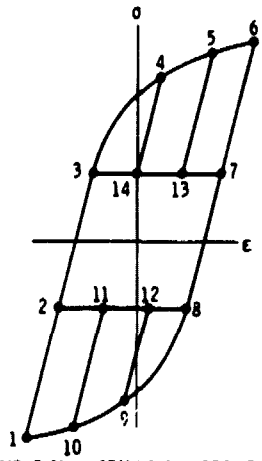

NUMBER OF TIMES EACH ELEMENT OF HYSTERESIS LOOPS IS TRAVERSED IN TWO TYPES OF ANALYSIS INHERENT IN INTERACTION DAMAGE RULE

NINE COMBINATIONS OF WAYS TO TRAVERSE LOOP TO ACHIEVE SAME EFFECT AS THREE BASIC LOOPS											THREE BASIC LOOPS			
PATH	A_1	B_1	C_1	A_2	B_2	C_2	A_3	B_3	C_3	TOTAL	3_A	3_B	3_C	TOTAL
1-2	0	1	1	0	1	1	0	1	1	6	3	0	3	6
2-3	1	1	1	1	1	1	1	1	1	9	3	3	3	9
3-4	1	1	1	0	0	0	0	0	0	3	3	0	0	3
4-5	0	0	0	1	1	1	0	0	0	3	3	0	0	3
5-6	0	0	0	0	0	0	1	1	1	3	3	0	0	3
6-7	0	0	0	0	0	0	1	1	1	3	3	0	0	3
7-8	1	1	1	1	1	1	1	1	1	9	3	3	3	9
8-9	1	1	0	1	1	0	1	1	0	6	3	0	3	6
9-10	1	0	1	1	0	1	1	0	1	6	3	0	3	6
10-1	0	1	1	0	1	1	0	1	1	6	3	0	3	6
3-14	0	0	0	1	1	1	1	1	1	6	0	3	3	6
14-13	1	1	1	0	0	0	1	1	1	6	0	3	3	6
13-7	1	1	1	1	1	1	0	0	0	6	0	3	3	6
6-12	0	0	1	0	0	1	0	0	1	3	0	3	0	3
12-11	0	1	0	0	1	0	0	1	0	3	0	3	0	3
11-12	0	1	0	0	1	0	0	1	0	3	0	3	0	3

Figure 26. - Number of times each element of hysteresis loops is traversed in two types of analysis inherent in interaction damage rule.

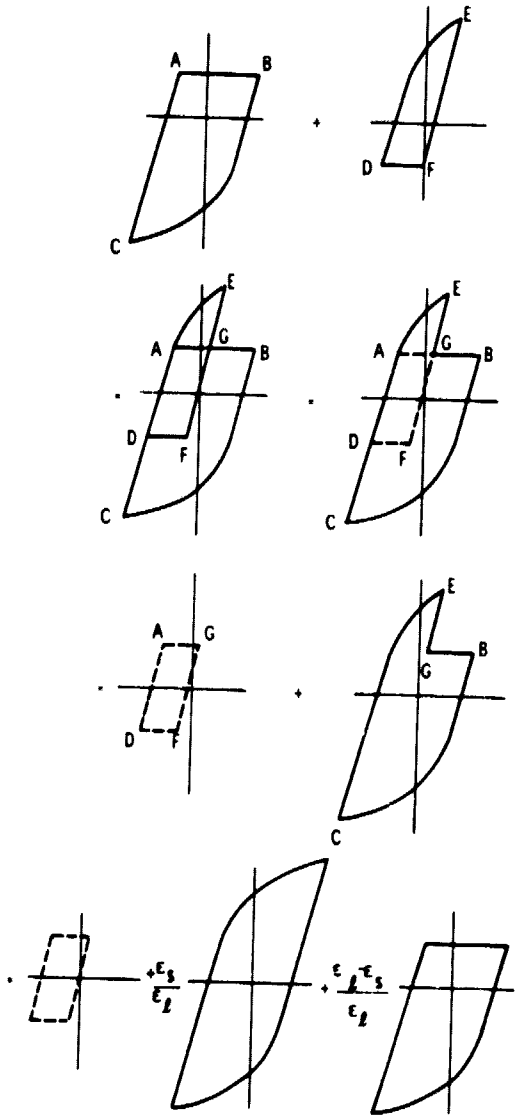

Figure 29. - Strainrange conversion for CP and PC loops of unequal amplitudes

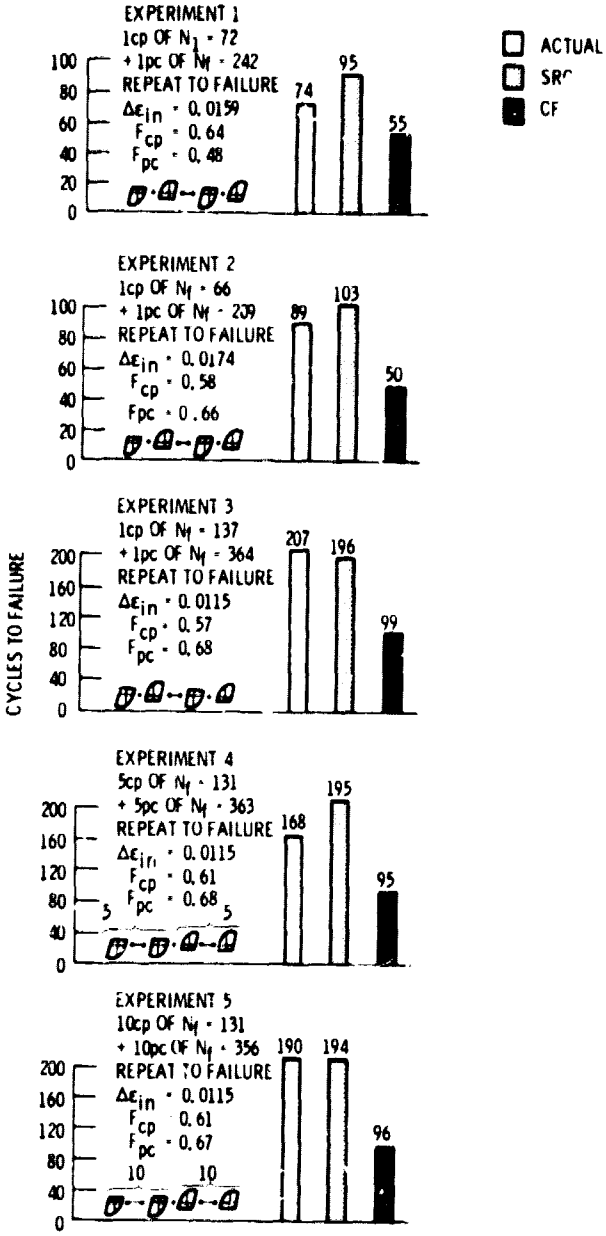

Critical experiments on 316 SS to validate high temperature fatigue mechanism according to strainrange conversion principle.

Figure 30. - Summary of strainrange conversion experiments involving equal strainranges of CP and PC types.

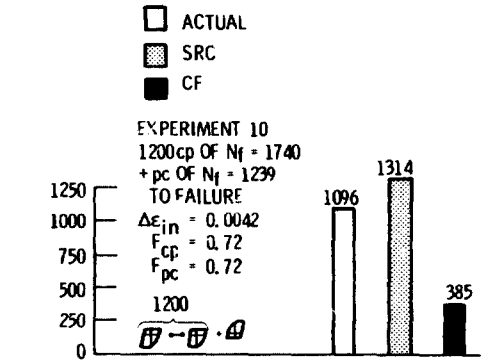

Check of SRC principle on 2 1/4 Cr-1 Mo by applying a series of initial cp loops and continuing to failure with pc loading to failure.

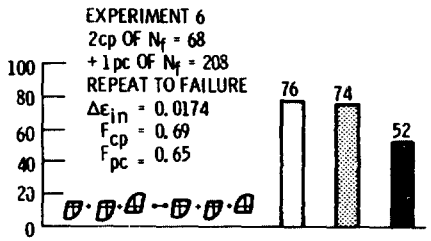

Check of the strainrange conversion principle on 316 SS using unequal numbers of cp and pc loops.

Figure 30. - Continued.

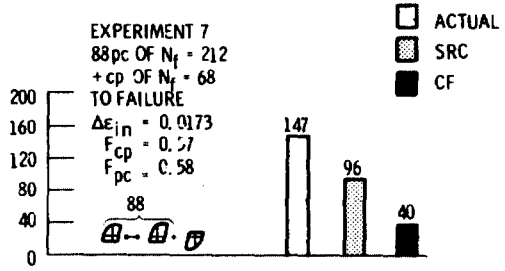

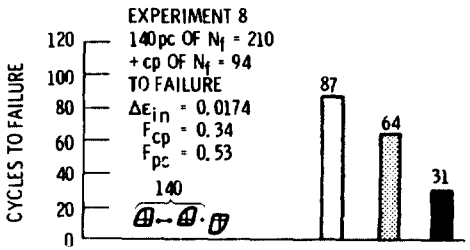

Check of SRC principle on 316 SS by applying a series of initial pc loops after which cp loops are applied until failure occurs.

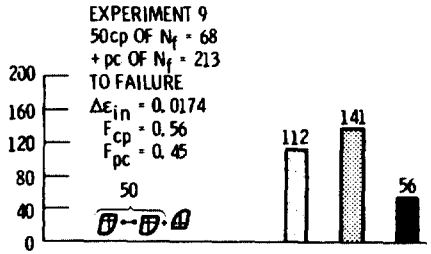

Check of SRC principle on 316 SS by applying a series of initial cp loadings after which pc loops are applied until failure occurs.

Figure 30. - Concluded.

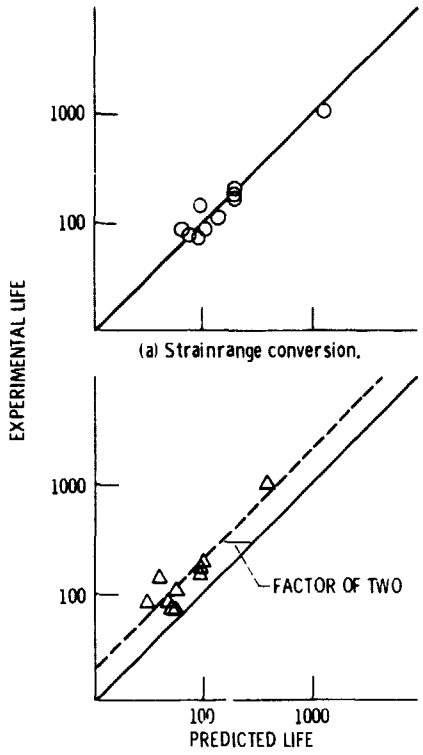

(b) Cycle fraction.

Figure 31. - Comparison of experimental results for critical experiments with calculations by Strainrange conversion and by cycle fraction rules.

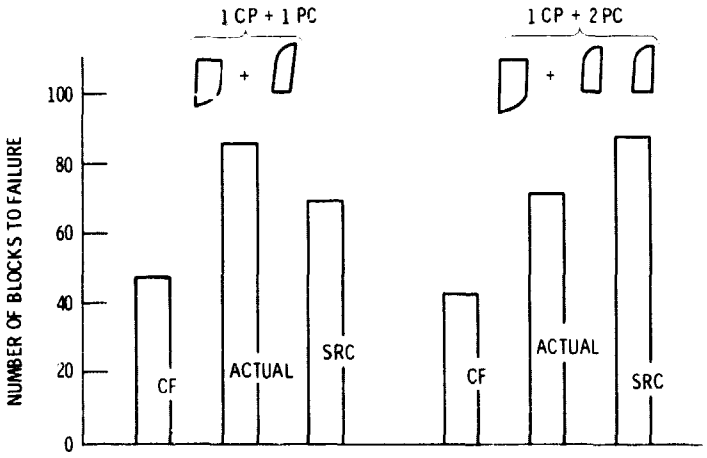

Figure 32. - Summary of results of SRC experiments involving unequal strainranges.

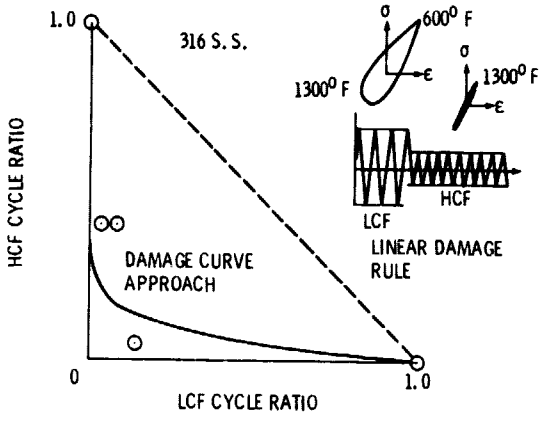

Figure 33. - HCF/LCF interaction at high temperature.

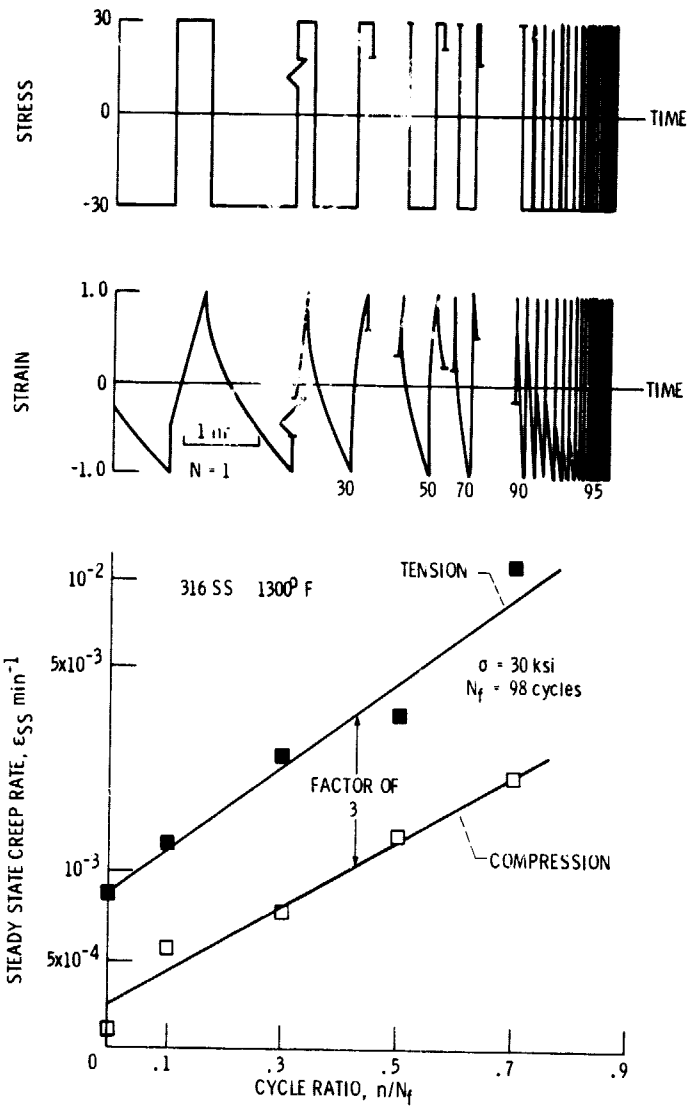

Figure 34. - Creep rate response in tension and compression of a cyclic creep rupture test.

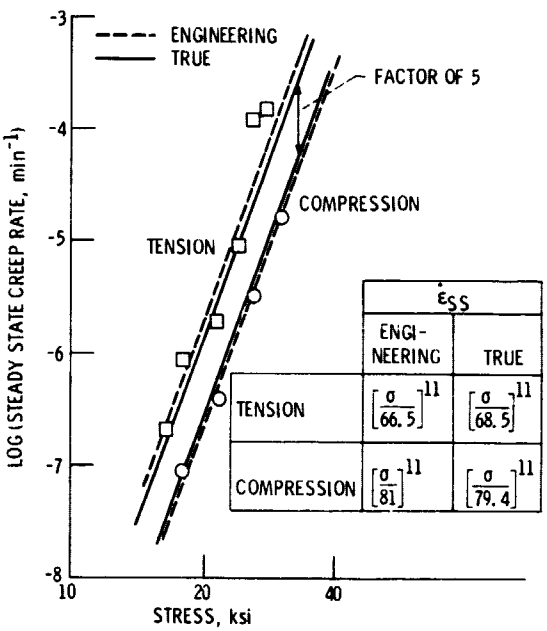

Figure 35. - Comparison of creep rates in tension and compression for 316 SS at 705 C(1300° F).